(20 kyr BP) sea-level lowstand gives 120 ± 5 m, in agreement with fossil reef results[1] and supporting our mean value for H_{crit}.

To evaluate the dependence of our lowstand reconstructions on the main assumption that previous glacial ΔS values were similar to LGM values of 10 ± 2 p.s.u., we perform two tests based on the highest extreme glacial salinity estimate (55 p.s.u.; ref. 11). One increases ΔS to 15 p.s.u.; the other keeps ΔS at 10 p.s.u. but increases its confidence interval ($d\Delta S$) from ± 2 to ± 5 p.s.u. In the first test, H_{crit} is smaller, and reconstructed sea level drops are greater, by a maximum of 6 m. In the second test, with $d\Delta S$ increased by a factor of 2.5, the lowstand confidence intervals remain accurate within a factor of 2 (Fig. 3). These results justify the use of the SBM uplift rate with H_{crit} to study pre-stage-6 lowstands, noting that our method is more likely to underestimate rather than overestimate past sea-level drops, by a few metres.

Accounting for uplift since stage 8 (270 kyr BP), sill depth was around 150 m b.p.s.l. Stage 8 does not contain a completely 'aplanktonic' interval. Although the total planktonic foraminiferal numbers are strongly reduced, the main species composition shows little change that might reflect high-salinity stress (Fig. 1). We infer that sill depth remained considerably greater than H_{crit}. To allow continuation of all observed planktonic species, Red Sea salinity should have remained below a maximum of ~45 p.s.u., requiring a minimum sill depth of ~30 m (compare ref. 14). Hence, the maximum conceived stage 8 sea level drop is $150 - 30 = 120$ m b.p.s.l.(± 8 m).

A similar argument to that for stage 8 may be made for stage 10 (340 kyr BP). However, stage 10 shows a much closer approximation of a complete 'aplanktonic' zone, with disruption of the main species composition. We infer that sill depth was maintained between H_{crit} (18 m) and 30 m, defining a stage 10 lowstand between 134 and 122 m b.p.s.l. (± 9 m).

Stage 12 (440 kyr BP) contains a true 'aplanktonic' zone (Fig. 1), suggesting a sill depth around H_{crit} and, consequently, a sea-level lowstand of 139 m b.p.s.l. (± 11 m). This mean value implies that global ice-volume during stage 12 exceeded LGM values by some 15%. This independently derived result validates the only previous estimate of stage 12 ice-volume, based on benthic oxygen-isotope records[5].

Our lowstand values allow assessment of sea-level rises during the main deglaciations of the past 500 kyr (Fig. 1i), for comparison with that of 120 m following the LGM[1]. With the maximum stage 5 sea level ~6 m above the present[2,6], the stage 6–5 sea-level rise was around 131 ± 6 m. During interglacial stage 7, sea level remained below the present-day level[4,5], giving a maximum amplitude for the stage 8–7 sea-level rise of 120 m, although the actual rise was probably considerably smaller. The stage 9 highstand reached 0–15 m above the present-day level[4,5], giving a stage 10–9 sea-level rise between 122 and 149 m. The largest sea-level rise of the past 500 kyr followed the stage 12 lowstand of 139 ± 11 m b.p.s.l. and culminated in a maximum stage 11 highstand up to 20 m above present-day sea level[21].

We conclude that the last glacial–interglacial cycle showed ice-volume fluctuations that were more than 10% smaller than those that occurred in three out of four of the immediately preceding main cycles. The stage 12–11 sea level rise implies that over 30% greater ice-volume changes were involved in Quaternary glacial–interglacial cycles than would be expected on the basis of the last cycle alone. □

1. Fairbanks, R. G. A 17,000 year glacio-eustatic sea level record: Influence of glacial melting rates on the Younger-Dryas event and deep ocean circulation. *Nature* **342**, 637–642 (1989).
2. Radtke, U. & Grün, R. Revised reconstruction of middle and late Pleistocene sea-level changes based on new chronologic and morphologic investigations in Barbados, West Indies. *J. Coastal Res.* **6**, 699–708 (1990).
3. Pirazzoli, P. A. *et al.* A one million-year-long sequence of marine terraces on Sumba Island, Indonesia. *Mar. Geol.* **109**, 221–236 (1993).
4. Bard, E. *et al.* Pleistocene sea levels and tectonic uplift based on dating of corals from Sumba Island, Indonesia. *Geophys. Res. Lett.* **23**, 1473–1476 (1996).
5. Shackleton, N. J. Oxygen isotopes, ice volume and sea level. *Quat. Sci. Rev.* **6**, 183–190 (1987).
6. Chappell, J. & Shackleton, N. J. Oxygen isotopes and sea level. *Nature* **324**, 137–140 (1986).
7. Berggren, W. A. & Boersma, A. in *Hot Brines and Heavy Metal Deposits* (eds Degens, E. T. & Ross, D. A.) 282–298 (Springer, 1969).
8. Halicz, E. & Reiss, Z. Palaeoecological relations of foraminifera in a desert enclosed sea—The Gulf of Aqaba. *Mar. Ecol.* **2**, 15–34 (1981).
9. Locke, S. & Thunell, R. C. Palaeoceanographic record of the last glacial-interglacial cycle in the Red Sea and Gulf of Aden. *Palaeogeogr. Palaeoclimatol. Palaeoecol.* **64**, 163–187 (1987).
10. Almogi-Labin, A., Hemleben, C., Meischner, D. & Erlenkeuser, H. Palaeoenvironmental events during the last 13,000 years in the central Red Sea as recorded by pteropoda. *Paleoceanography* **6**, 83–98 (1991).
11. Hemleben, C. *et al.* Three hundred and eighty thousand year long stable isotope and faunal records from the Red Sea: Influence of global sea level change on hydrography. *Paleoceanography* **11**, 147–156 (1996).
12. Milliman, J. D., Ross, D. A. & Ku, T. L. in *Hot Brines and Heavy Metal Deposits* (eds Degens, E. T. & Ross, D. A.) 724–736 (Springer, New York, 1969).
13. Ku, T. L., Thurber, D. L. & Mathieu, G. G. in *Hot Brines and Heavy Metal Deposits* (eds Degens, E. T. & Ross, D. A.) 348–359 (Springer, New York, 1969).
14. Rohling, E. J. Glacial conditions in the Red Sea. *Paleoceanography* **9**, 653–660 (1994).
15. Rohling, E. J. & Zachariasse, W. J. Red Sea outflow during the last glacial maximum. *Quat. Int.* **31**, 77–83 (1996).
16. Werner, F. & Lange, K. A bathymetric survey of the sill area between the Red Sea and Gulf of Aden. *Geol. Jahrb. D* **13**, 125–130 (1975).
17. Siedler, G. in *Hot Brines and Heavy Metal Deposits* (eds Degens, E. T. & Ross, D. A.) 131–137 (Springer, New York, 1969).
18. Rohling, E. J., Jorissen, F. J., Vergnaud-Grazzini, C. & Zachariasse, W. J. Northern Levantine and Adriatic Quaternary planktic foraminifera; Reconstruction of paleoenvironmental gradients. *Mar. Micropaleontol.* **21**, 191–218 (1993).
19. Ganssen, G. & Kroon, D. Evidence for Red Sea surface circulation from oxygen isotopes of modern surface waters and planktonic foraminiferal tests. *Paleoceanography* **6**, 73–82 (1991).
20. Squires, G. L. *Practical Physics* 3rd edn (Cambridge Univ. Press, 1988).
21. Howard, W. R. A warm future in the past. *Nature* **388**, 418–419 (1997).
22. Imbrie, J. *et al.* in *Milankovitch and Climate* (eds Berger, A. *et al.*) 269–305 (Reidel, Hingham, MA, 1984).

Megaripple migration in a natural surf zone

Edith L. Gallagher*, Steve Elgar† & Edward B. Thornton*

* *Oceanography Department, Naval Postgraduate School, Monterey, California 93943, USA*
† *School of Electrical Engineering and Computer Science, Washington State University, Pullman, Washington 99164, USA*

Migrating megaripples are bedforms that appear in the surf zone of sandy coasts[1]. With heights of 0.1–0.5 m and wavelengths of 1–5 m, they are similar in size and shape to small dunes, large ripples, or sand waves. Such sedimentary bedforms have been studied in subaerial[2], steady-flow[3] and intertidal[4] environments, as well as in laboratory flume experiments[5]. They affect overlying currents by introducing hydraulic roughness[4,6], and may provide a mechanism for sediment transport[7,8] as well as forming sedimentary structures in preserved facies[9,10]. The formation, orientation and migration of such bedforms is not understood well[11,12]. Dunes, for example, can be aligned with their crests perpendicular to steady unidirectional winds[13], but in more complex wind fields their orientation becomes difficult to predict[14–17]. Similarly, it is not known how sea-floor megaripples become aligned and migrate in the complex flows of the surf zone. Here we present observations in the surf zone of a natural beach which indicate that megaripples do not migrate in the direction of the vector sum of the currents, but are aligned so that the sediment transport normal to the bedform crest is maximized[17]. This may need to be taken into account in modelling morphology change and interpreting existing and fossil morphologic patterns.

Lunate-shaped megaripples migrating shoreward have been observed by scuba divers in a high-energy surf zone on the Oregon coast[1] and with sonar images of the sand bed in the surf zone of a large lake during the waning stages of a storm[18]. Onshore migration has been proposed to result from sediment transport associated with asymmetries in wave velocities[19], but migration with steady unidirectional flows (rip, longshore and tidal currents) has also been observed[20–23]. We have made observations in the surf zone of a natural beach (Fig. 1a) with an array of seven downward-looking sonar altimeters[24] that measure the distance to the sea floor from a fixed frame (Fig. 1b). Megaripples (often visually determined to be slightly lunate shaped) were present about 60% of the time during the six-week experiment, which included a wide range of wave heights (from 0.1 to 4.0 m) and mean currents (from 0 to 2 m s^{-1}). An example of migrating megaripples is shown in Fig. 2.

To determine migration rate and direction quantitatively, we used time domain cross correlation to calculate the time lag (Δt) of maximum correlation between sensor pairs, separated by distances Δx and Δy in the cross- and alongshore directions, respectively. The components of megaripple migration velocity ($\Delta x/\Delta t$, $\Delta y/\Delta t$) calculated from each sensor pair (when the maximum correlation was greater than 0.4) were averaged, giving an estimate of cross- (U_{Mrip}) and along shore (V_{Mrip}) migration speed and direction $\theta_{Mrip} = \text{atan}(V_{Mrip}/U_{Mrip})$. Average (over 48 h) migration speeds range from 0.1 to 1.7 m h^{-1}.

The measured cross- and alongshore fluid velocities (Fig. 1) were separated into mean and fluctuating (that is, wave) components and 48-h mean cross- ($\bar{U}_{48}$) and alongshore ($\bar{V}_{48}$) velocities were calculated. The direction of the 48-h mean current $\theta_{mean} = \text{atan}(\bar{V}_{48}/\bar{U}_{48})$ was rarely aligned with the direction of megaripple migration, θ_{Mrip} (Fig. 3a). Megaripples were aligned with the alongshore ($\sim 90°$ in Fig. 3a) steady flow ($\bar{V}_{48}$) only during periods when $\bar{V}_{48}$ was relatively large (more than about 1.5 times the root-mean-square (r.m.s.) wave velocity and $\bar{V}_{48} \gg \bar{U}_{48}$).

Hourly skewness-weighted r.m.s. cross- ($\langle \tilde{u}^3 \rangle / \langle \tilde{u}^2 \rangle$) and along-shore ($\langle \tilde{v}^3 \rangle / \langle \tilde{v}^2 \rangle$) wave velocities, where $\tilde{u}$, $\tilde{v}$ are the cross- and alongshore components of the fluctuating velocities, respectively and $\langle \rangle$ denote time average, were averaged to give 48-h cross- ($\tilde{U}_{48}$) and alongshore ($\tilde{V}_{48}$) wave velocities with magnitude $\sqrt{\tilde{U}_{48}^2 + \tilde{V}_{48}^2}$ and direction $\theta_{wave} = \text{atan}(\tilde{V}_{48}/\tilde{U}_{48})$. The skewness-weighted r.m.s. is used because it represents the magnitude of the wave velocities, similar to the r.m.s. velocity, as well as the direction of the onshore skewed waves in the surf zone, believed to be important to net sediment transport[25]. Megaripples were most closely aligned with the onshore ($\sim 0°$ in Fig. 3b) directed wave velocities (consistent with previous visual observations[1,18,19]) when the mean currents were relatively small. However, in general the r.m.s. difference between θ_{Mrip} and θ_{wave} is large and θ_{wave} cannot be used to predict θ_{Mrip} (Fig. 3b).

Megaripple migration direction also is not correlated with the direction of the vector sum of the mean and wave velocities $\theta_{total} = \text{atan}((\bar{U}_{48} + \tilde{U}_{48})/(\bar{V}_{48} + \tilde{V}_{48}))$ (Fig. 3c). Comparison of the migration directions with θ_{total} (Fig. 3c) indicates that these observations include transverse, longitudinal and oblique bedforms[26].
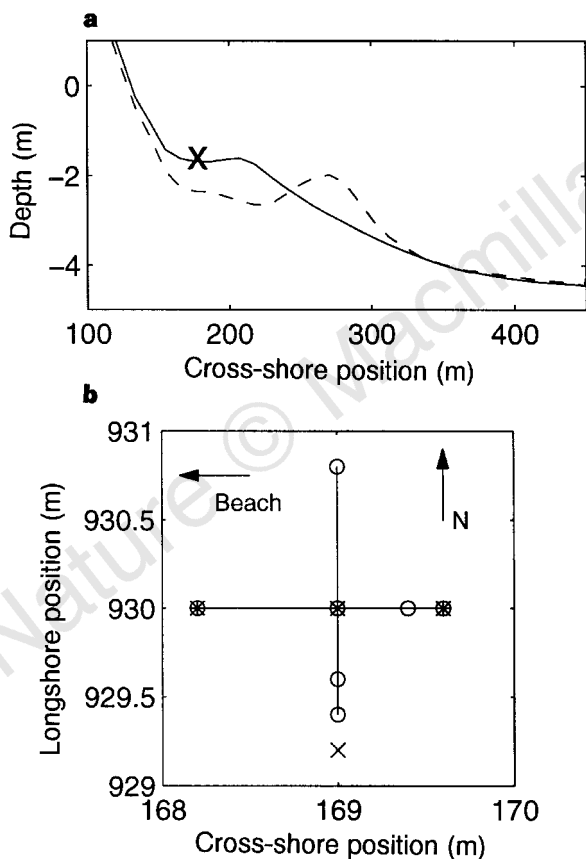

Figure 1 Location of the altimeter array in the surf zone. **a**, Depth of the sea floor (relative to mean sea level) versus cross-shore position. Profiles from the start (1 Sep, solid curve) and end (14 Oct, dashed curve) of the observation period are shown. The array was located ~50 m from the shoreline in the trough (X) between the sandbar and the beach on a barrier island exposed to the Atlantic Ocean near the town of Duck, North Carolina, USA. The mean water depth at the array ranged from 1.5 to 2 m between 1 September and 14 October 1994 as the large-scale beach morphology evolved. The amplitude of the semidiurnal tide near Duck is about 0.5 m and the mean sand-grain diameter near the array was ~0.2 mm. **b**, Plan view of the altimeter array. Circles represent locations of individual altimeters (time series from those with asterisks are shown in Fig. 2) and the cross shows the location of an electromagnetic current meter that measured cross- and alongshore components of the fluid velocity field every 0.5 s about 0.5 m above the sea floor.
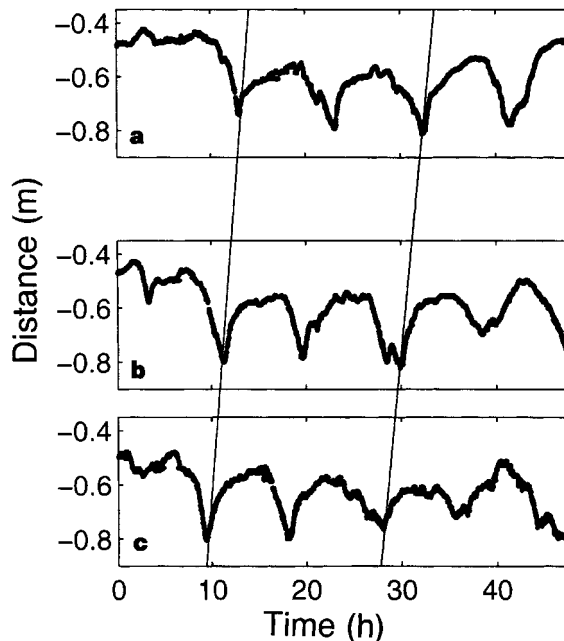

Figure 2 Distance to the sea floor (every 32 s (ref. 24) for 48 h) from three altimeters (circled asterisks in Fig. 1b) versus time. The altimeters were separated in the cross-shore direction by 80 (upper (**a**) to middle (**b**) panel) and 60 cm (middle (**b**) to lower (**c**) panel) and the panels are separated accordingly. Time series in the top panel are from the most onshore altimeter. The slopes of the lines connecting the 'troughs' of the bedforms illustrate onshore migration of the features (~0.3 m h^{-1}).

A similar lack of alignment of subaerial bedforms with the resultant transport vector in quasi-steady but directionally changing flows has been observed previously[17,27]. Experiments in which a large sand-covered table was rotated periodically in steady wind led to the hypothesis that bedforms are not aligned with the resultant transport vector **R**, but so that the gross sediment transport $T = |T_S| + |T_D|$ (Fig. 4a) normal to their crests is maximized[17]. Using gross transport allows back-and-forth motion of the sand to build a feature even if the net transport across the bedform is zero. For bidirectional flows, the orientation α of the bedform, relative to

the dominant transport vector **D**, which maximizes the sum of the absolute value of bedform-normal components of the transport vectors $T = D|\sin\alpha| + S|\sin(\gamma - \alpha)|$, where **S** is the subordinate transport vector at angle γ relative to **D** (Fig. 4a), is given by[17]

$$\tan\alpha = \pm \frac{|D|/|S| + |\cos\gamma|}{|\sin\gamma|} \tag{1}$$

Equation (1) is applicable when the durations of the two temporally distinct transport vectors (**D** and **S**) are each short enough that the bedforms do not come into equilibrium with either transporting flow[28]. In the mixed flows on a natural beach, mean and wave velocities act simultaneously and thus cannot be used to represent **D** and **S**. However, the opposing oscillatory flows, modified in amplitude and direction by mean currents, are temporally distinct. The periods (order 10 s) of the wave velocities are far shorter than the time required for megaripples to equilibrate, so equation (1) is valid.

In a natural surf zone, there is large range in the magnitude and direction of individual waves, and thus the bidirectional solution
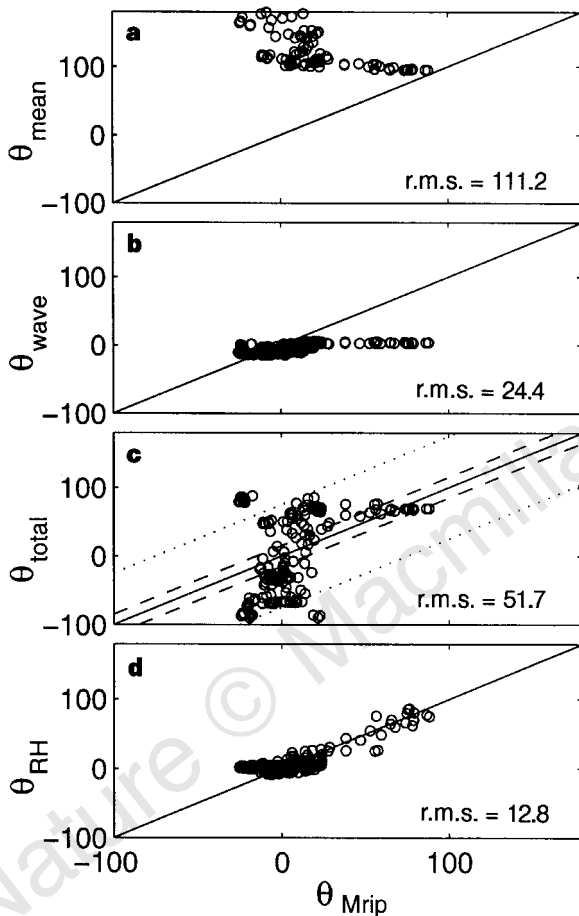

Figure 3 Direction of fluid flow versus megaripple migration. Direction of **a**, mean current; **b**, wave velocity; **c**, vector sum of mean and wave velocities; and **d**, bedform orientation (θ_{RH}) predicted by maximizing the gross, bedform-normal transport T (equation (2))[17] versus observed megaripple migration direction (in degrees with 0° onshore and 90° to the south). All values are 48-h averages, which include enough migrating features for statistical stability, while retaining stationarity of the slowly evolving bedforms. The features change constantly, so overlapping 48-h estimates starting every 3 h were used. Changing the size of the averaging period or the overlap by a factor of 2 does not strongly affect the results presented here. The root-mean-square (r.m.s.) difference between the dependent variable and the observed megaripple migration direction (θ_{Mrip}) is listed in each panel. The r.m.s. differences between θ_{RH} and θ_{Mrip} (12.8) are smaller than those between θ_{Mrip} and the directions of the mean current (111.2), the wave-orbital velocities (24.4), or their resultant (51.7). In **c**, the broken lines delineate regions occupied by traditional bedform classes[26]. Transverse bedforms (0° ≤ |θ_{total} − θ_{Mrip}| < 15°) fall inside the dashed lines, longitudinal bedforms (75° < |θ_{total} − θ_{Mrip}| ≤ 90°) fall outside the dotted lines and oblique bedforms (75° < |θ_{total} − θ_{Mrip}| ≤ 75°) fall in between. The correlation between θ_{RH} and θ_{Mrip} (**d**) is $r = 0.86$, and changing the exponent of the velocity (that is, the model for sediment transport) from three to one or six results in correlations of $r = 0.85$ and $r = 0.87$, respectively. None is statistically different at the 99% level.
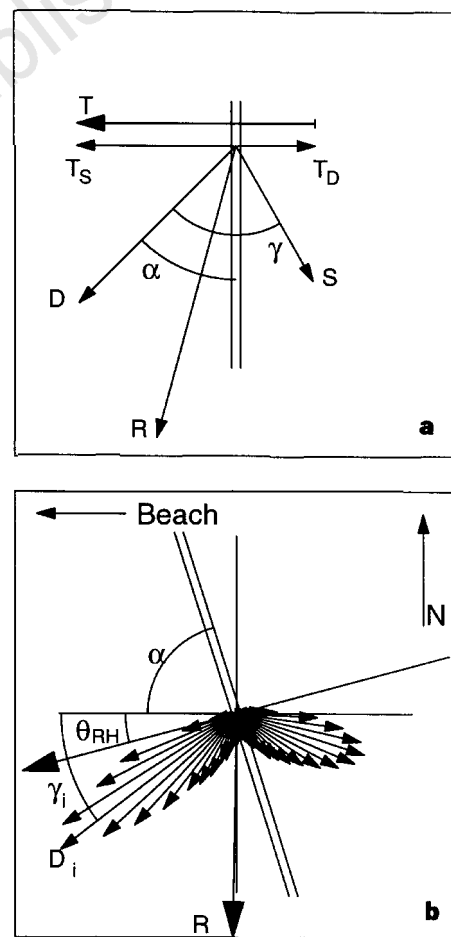

Figure 4 Transport vectors and bedform orientation[17]. **a**, Following ref. 17, the angle between the dominant (*D*) and subordinate (*S*) transport vectors is γ, the angle between *D* and the bedform crest (double line) is α, *R* is the vector sum of *D* and *S*, and $T = |T_S| + |T_D|$ is the gross bedform-normal transport. **b**, Example of the directional distribution of cumulative transport (summed over a 3-h period) from instantaneous velocities in the surf zone (small arrows). The magnitude and direction of each cumulative transport vector are given by D_i and γ_i, respectively. The orientation of the bedform crest (double line) α is such that the gross bedform-normal transport T (equation (2)) is maximized. R shows the direction of the resultant vector for this example. Observed megaripple migration directions θ_{Mrip} are compared with $\theta_{RH} = 90° - \alpha$ in Fig. 3d.

(equation (1)) is modified to a sum over a continuum of instantaneous transport vectors, with the component of gross transport normal to the bedforms given by

$$T = \sum_i D_i |\sin(\gamma_i - \alpha)| \qquad (2)$$

where i ranges over all transport vectors. Although in this more general case of many transport vectors there is no analytical solution for α, the gross, bedform-normal transport T can be maximized numerically to give bedform orientation.

In the bidirectional, rotating table experiments[17], transport vectors **D** and **S** were proportional to the duration of steady winds in each direction, and thus the bedform orientation α depended on the ratio $|\mathbf{D}|/|\mathbf{S}|$ (equation (1)) and not on a particular sediment transport model. However, the more general solution requires a sediment transport model to represent D_i. Similar to bedload models[25], D_i was calculated as proportional to the instantaneous velocity cubed. The results are not sensitive to the exponent of the velocity used to calculate D_i. Here, the individual instantaneous (2 Hz) transport vectors (calculated from velocity measurements) were summed over a 3-h period and sorted into 5°-wide directional bins, giving a directional distribution of cumulative transport (see, for example, Fig. 4b). The distribution was used to calculate T (equation (2)), with γ_i and D_i equal to the direction and corresponding magnitude of the cumulative transport in each bin. The value of α for which T is maximum was then found for each 3-h period. The model is sensitive to the estimation period and better results were obtained with shorter periods, implying that the bedforms respond quickly (order 3 h) to changes in the flow field.

For comparison with megaripple migration direction observations, 16 sequential 3-h estimates of α were averaged to give a 48-h estimate. Assuming that megaripples migrate ~90° to their crest orientation, a predicted migration direction is given by $\theta_{RH} = 90° - \alpha$. As shown in Fig. 3d, θ_{RH} predicts accurately the observed megaripple migration direction θ_{Mrip} (the slope (1.04) of a best-fit line does not differ significantly from 1.00 at the 99.5% level).

These observations suggest that megaripple migration in the surf zone is caused by both mean and wave flows. However, the migration direction is not aligned with the vector sum of the currents, but so that gross sediment transport normal to the bedform is maximized, as suggested previously for subaerial features[17]. Megaripples in the surf zone of a natural barred beach occur frequently for a wide range of wave and current conditions, and include transverse, longitudinal and oblique bedforms. If migration of bedforms is an important mechanism for bedload sediment transport, parametrizations that depend only on waves, currents, or even their vector sum, may not predict the observed transport accurately. Conversely, flow conditions inferred from alignment of bed features preserved in ancient sedimentary deposits or observed in modern environments may not be unique because different flow fields can maximize gross bedform-normal transport. □

1. Clifton, H. E., Hunter, R. E. & Phillips, R. L. Depositional structures and processes in the non-barred high-energy nearshore. *J. Sedim. Petrol.* **41,** 651–670 (1971).
2. Bagnold, R. A. *The Physics of Wind Blown Sand and Desert Dunes* (Methuen, London, 1954).
3. Simons, D. B. & Richardson, E. V. Forms of bed roughness in alluvial channels. *Am. Soc. Civ. Eng. Trans.* **128,** 284–302 (1963).
4. Dalrymple, R. W., Knight, R. J. & Lambiase, J. J. Bedforms and their hydraulic stability relationships in a tidal environment, Bay of Fundy, Canada. *Nature* **275,** 100–104 (1978).
5. Southard, J. B., Lambie, J. M., Federico, D. C., Pile, H.T. & Weidman, C. R. Experiments on bed configurations in fine sands under bidirectional purely oscillatory flow, and the origin of hummocky cross-stratification. *J. Sedim. Petrol.* **60,** 1–17 (1990).
6. Garcez Faria, A. F., Thornton, E. B., Stanton, T. P., Soares, C. V. & Lippmann, T. C. Vertical profiles of longshore currents and related bed shear stress and bottom roughness. *J. Geophys. Res.* **103,** 3217–3232 (1998).
7. Allen, J. R. L. *Current Ripples: Their Relation to Patterns of Water and Sediment Motion* (North-Holland, Amsterdam, 1968).
8. Middleton, G. V. & Southard, J. B. *Mechanics of Sediment Movement.* (Lecture for short course no. 3, Society of Economic Paleontologists and Mineralogists, 1982).
9. Davidson-Arnott, R. G. D. & Greenwood, B. Facies relationships on a barred coast, Kouchibouguac
Bay, New Brunswick, Canada. *Beach and Nearshore Sedimentation, SEPM Special Pub.* **24,** 149–169 (1976).
10. Sherman, D. J. & Greenwood, B. Hummocky cross-stratification and post-vertex ripples: length scales and hydraulic analysis. *Sedimentology* **36,** 981–986 (1989).
11. Werner, B. T. Eolian dunes: computer simulations and attractor interpretation. *Geology* **23,** 1107–1110 (1995).
12. Stam, J. M. T. On the modelling of two-dimensional aeolian dunes. *Sedimentology* **44,** 127–141 (1997).
13. Bagnold, R. A. Journeys in the Libyan Desert 1929 and 1939. *Geogr. J.* **78,** 13–39 (1933).
14. Warren, A. Dune trend and the Ekman spiral. *Nature* **259,** 653–654 (1976).
15. Tsoar, H. Dynamic processes operating on a longitudinal (seif) sand dune. *Sedimentology* **30,** 567–578 (1983).
16. Hanna, S. R. The formation of longitudinal sand dunes by large helical eddies in the atmosphere. *J. Appl. Meteorol.* **8,** 874–883 (1969).
17. Rubin, D. M. & Hunter, R. E. Bedform alignment in directionally varying flows. *Science* **237,** 276–278 (1987).
18. Hay, A. E. & Wilson, D. J. Rotary sidescan images of nearshore bedform evolution during a storm. *Mar. Geol.* **119,** 57–65 (1994).
19. Clifton, H. E. Wave-formed sedimentary structures-a conceptual model. *Beach and Nearshore Sedimentation, SEPM Special Pub.* **24,** 126–148 (1976).
20. Moore, J. N., Fritz, W. J. & Futch, R. S. Occurrence of megaripples in a ridge and runnel system, Sapelo Island, Georgia: morphology and processes. *J. Sedim. Petrol.* **54,** 615–625 (1984).
21. Sherman, D. J., Short, A. D. & Takeda, I. Sediment mixing depth and bedform migration in rip channels. *J. Coastal Res.* **15,** 39–48 (1993).
22. Dalrymple, R. W. & Rhodes, R. N. Estuarine dunes and barforms. *Dev. Sedimentol.* **53,** 359–422 (1995).
23. Hay, A. E. & Bowen, A. J. Alongshore migration of lunate megaripples during DUCK94. *J. Geophys. Res.* (in the press).
24. Gallagher, E. L., Boyd, W., Elgar, S., Guza, R. T. & Woodward, B. Performance of a sonar altimeter in the nearshore. *Mar. Geol.* **133,** 241–248 (1996).
25. Bagnold, R. A. An approach to the sediment transport problem from general physics. *US Geol. Surv. Prof. Paper* **422-I** (1966).
26. Rubin, D. M. Cross-bedding, bedforms, and paleocurrents: Concepts in sedimentology and paleontology. *SEPM Special Pub.* **1** (1987).
27. Fryberger, S. G. Dune forms and wind regime. *A Study of Global Sand Seas, Pap. US Geol. Surv.* **1052,** 137–170 (1979).
28. Rubin, D. M. & Ikeda, H. Flume experiments on the alignment of transverse, oblique, and longitudinal dunes in directionally varying flows. *Sedimentology* **37,** 673–684 (1990).

The unique anisotropy of the Pacific upper mantle

Göran Ekström & Adam M. Dziewonski

Department of Earth and Planetary Sciences, Harvard University, 20 Oxford Street, Cambridge, Massachusetts 02138, USA

The development and interpretation of tomographic models of the Earth's mantle have usually proceeded under the assumption that fast and slow seismic velocity anomalies represent a spatially heterogeneous temperature field associated with mantle convection. Implicit in this approach is an assumption that either the effect of anisotropy on seismic velocities is small in comparison with isotropic thermal or compositional effects, or that the tomographic results represent the average isotropic heterogeneity, even if individual seismic observations are affected by anisotropic structure. For example, velocity anomalies in the upper portions of the oceanic mantle are commonly interpreted in terms of the progressive cooling[1,2] (and localized reheating[3]) of a mechanical and thermal boundary layer consisting of rigid oceanic lithosphere and an underlying, less viscous, asthenosphere. Here, however, we present results from a global three-dimensional tomographic model of shear-wave velocity which shows that the uppermost mantle beneath the central Pacific Ocean is considerably more complicated than this simple model. Over a broad area, with its centre near Hawaii, the seismic data reveal a regional anomaly in elastic anisotropy which produces variations of seismic velocities that are at least as large as